Wet steam flow in 1100 MW turbine

GUKCHOL JUN[a,b]
MICHAL KOLOVRATNÍK[b]
MICHAL HOZNEDL[a*]

Czech Technical University in Prague, Technická 4, 160 00, Prague, Czech Republic
Doosan Škoda Power s.r.o., Tylova 1/57, 301 28, Pilsen, Czech Republic

Abstract The paper deals with the wet steam flow in a steam tur-bine operating in a nuclear power plant. Using a pneumatic and an optical probe, the static pressure, steam velocity, steam wetness and the fine water droplets diameter spectra were measured before and beyond the last turbine low-pressure stage. The results of the experiment serve to understand better the wet steam flow and map its liquid phase in this area. The wet steam data is also used to modify the condensation model used in computational fluid dynamics simulations. The condensation model, i.e. the nucleation rate and the growth rate of the droplets, is adjusted so that results of the nu-merical simulations are in a good agreement with the experimental results. A 3D computational fluid dynamics simulations was performed for the low-pressure part of the turbine considering non-equilibrium steam condensa-tion. In the post-processing of the of the numerical calculation result, the thermodynamic wetness loss was evaluated and analysed. Loss analysis was performed for the turbine outputs of 600, 800, and 1100 MW, respectively.

Keywords: Steam turbine; Wet steam loss; Non-equilibrium condensation; CFD

Nomenclature

c – velocity, $m \cdot s^{-1}$
D_{32} – Sauter mean diameter od droplets, m
Δh_i – thermodynamic wetness loss in the individual domains (blade rows, i = 1 to 6), $kJ \cdot kg^{-1}$
J – nucleation rate, $m^{-3} \cdot s^{-1}$
L – specific enthalpy of evaporation, $J \cdot kg^{-1}$
$\dot{m}$ – steam mass flow, $kg \cdot s^{-1}$
N – output, MW
p – pressure, MPa, Pa
r – droplet radius, m
r_* – critical droplet radius, m
T – temperature, K
ΔT – subcooling, K
t – time, s
u – circumferential velocity on mid blading diameter, $m \cdot s^{-1}$
y – wetness, 1
θ – circumferential position in calculated domain, °

Subscripts

A, B – adjustment coefficients
l – liquid
g – gas
L-0 – last stage
L-1 – 2nd stage from the outlet
L-2 – 3rd stage from outlet
L-3 – 4th stage from outlet
sat – saturated
EQ – equilibrium
NEQ – non-equilibrium
in – inlet
x – axial direction
0 – condition (plane) before L-0 stage
1 – condition (plane) after stator blades of L-0 stage
2 – condition (plane) after L-0 stage
α – absolute steam flow angle

Acronyms

Au – gold
CFD – computational fluid dynamics
CTU – Czech Technical University
LP – low pressure
LSB – last stage blade
RB – rotor blades
SB – stator blades

1 Introduction

Research into the flow of wet steam in steam turbines and the interac-tion of its liquid phase with the flow path has long been carried out both on the basis of experiments [1–5] and using numerical simulations [6–8]. It focuses on understanding negative erosion mechanisms caused by coarse water droplets and additional energy losses of steam wetness which are determined mainly by the conditions of formation and development, quantity, spectrum of diameters and velocities of primary fine water droplets. The aim of the research is to consider the negative effects associated with water droplets in the design of turbine stages and to minimize them as much as possible. In the Czech Republic, the steam turbine manufacturer Doosan Škoda Power and Czech Technical University in Prague (CTU) have been cooperating for a long time to solve this problem. One of the co-research areas is modelling and quantification of additional energy losses in the specific geometry of the steam turbine and for various operational modes of the turbine. The thermodynamic wetness loss is one of the most important additional losses [9–12]. The thermodynamic wetness loss is defined by the degree of irreversible heat and mass transfer between the gaseous phase of the steam and primary water droplets [13].

The paper shows the possibilities of application of commercial software for turbomachinery applications Ansys CFX in modeling 3D steam flow regarding non-equilibrium phase transition in low pressure (LP) part of steam turbine in a nuclear power plant with nominal output of 1100 MW from Doosan Škoda Power production. The used numerical model of the formation and development of the liquid phase along the steam flow path is modified based on experimental data. Specifically, the distribution of primary wetness and static pressure along the length of the blades before and after the last stage (L-0) of the LP part of the turbine is used to modify the model. These data are obtained from measurements in the power plant using various probes. However, this experimental process is technically and financially very demanding [14]. Therefore, this process is not yet widely used.

Using numerical simulations, some parameters can be obtained directly to evaluate the effect of wet steam on turbine efficiency. One of them is the thermodynamic wetness loss. Thanks to the numerical simulations, it is possible to identify the area of generation of the thermodynamic wetness loss and its intensity in different parts of the steam turbine. Simulations performed for different operating modes of the turbine then provide a more comprehensive view of the thermodynamic wetness loss mechanism.

2 Steam turbine description

This paper deals with a 1100 MW steam turbine, which is installed in a nuclear power plant in the Czech Republic. Thanks to the gradual modernization of high-pressure and three LP parts together with an increase in the thermal output of the reactor by 4%, an increase in output of 90 MW was achieved. During the modernization of the turbine, a new LP part was installed with a newly designed geometry of flow path together with steel rotor blades of the last stage blade (LSB) with a length of 1220 mm, lo-cated on the hub diameter of 1880 mm [15, 16]. The rotational speed of the turbine is 3000 rpm. The cross section at the outlet of the last blade row is 12 m^2. Thanks to larger flow cross-section of the new LP part and instalation of the longer LSB into the existing casing, the cross-section in the outlet case [17, 18] is reduced. Therefore, the pressure drop in the flow section between the LSB and the condenser could increase. However, a pos-sible increase in this loss is eliminated both by the installation of blades with better efficiency and by a lower axial speed [19] at the output than that for the turbine before the modernization [20].

3 Experimental setup

The LP part of the turbine was equipped with 4 passages for traversing of the pneumatic and optical probe. For better mapping of pressure losses along the steam flow path in the area of the last stage, the exhaust hood and the condenser neck, there are 26 static pressure taps. In addition to the measured values from these measuring points, other data were available, measured using the turbine control system.

Passages for probe traversing of diameter 50 mm were placed before and behind the last turbine stage at two circumferentially different places. Their places were on the left and the right side of the turbine, always 45° above the dividing plane. In plane 0 the probe axis was about 70 mm from the trailing edge of the rotor blade of the L-1 stage and inclined 10° from the vertical axis. In plane 2 the probe axis was about 120 mm behind the trailing edge of rotor balde of the L-0 stage. The inclination of the probe axis from the vertical axis was in this case 5° due to technical restrictions inside and outside the turbine. The flow part section with marking the axis position of both probes is shown in Fig. 1.

To define the distribution of static pressure and other flow parameters a pneumatic multi-hole disk probe was used. The probe calibration was

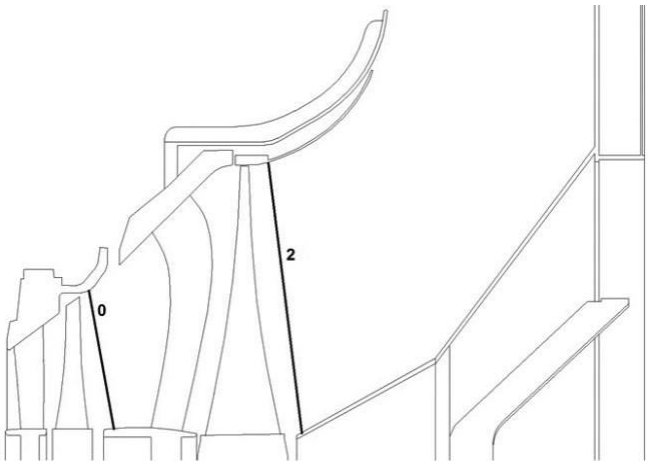

Figure 1: Flow part section and position of traversing planes 0 and 2 for probes.

performed in the wind tunnel designed for Mach number less than 0.7. Measurement was carried out from the root to the tip of blades with the traversing step of 25 mm in plane 0 and 50 mm in plane 2 respectively. In the area behind the part-span-connector installed on the LSB, it was possible to reduce the traversing steps of the probe. During the measure-ment, the pressure inside the condenser changed by a maximum of 100 Pa due to a change in the condenser cooling water temperature. All holes of the pneumatic probe were purged with a small amount of dry air to prevent water droplets from entering the pressure pipes and clogging the impulse tubes.Thanks to blowing of the probe by dry air, values of pres-sure were measured with an error of about 7–10 Pa. The amount of dry air was controlled by needle valves and flow meters. At each measuring point, the probe was manually balanced in the steam flow direction. Specifically, the probe was rotated until the pressure difference between the left and right taps at the front of the disk was less than 10 Pa. At this point, the distance of the disk from the heel and the angle of rotation of the probe, which corresponded to the angle α_2, were digitally measured. During further data processing, it was necessary to recalculate the velocity components determined in the probe coordinate system, see Fig. 2, into the turbine coordinate system. Both, pneumatic and optical probe are depicted in this picture.

The distribution of the outlet angle α_2 and static pressure along the blade length in planes 0 and 2 on both sides of the turbine were used as

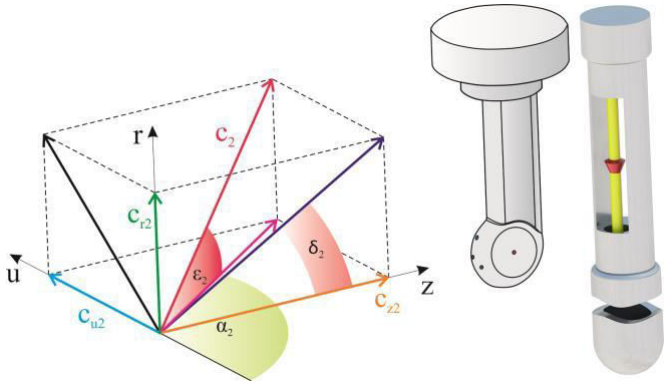

Figure 2: Marking of steam flow angles and velocity components.

input data for the traversing of an optical probe. Due to independent measurement of static pressure and steam wetness it was necessary to iterate the measurement results obtained using both probes. The agreement between pressure and wetness was reached usually after the second iteration.

The CTU optical measuring system was used to determine the structure of the liquid phase, i.e. the dimensions and the number of drops. Using the optical probe, the multispectral extinctions of light on fine water droplets of wet steam flowing through the measuring space of the probe is recorded at the measuring points of the probe. Therefore, the measured values by the optical probe are local. More comprehensive information of the liquid phase structure can be obtained by repeated measuring in the series of radial positions along the probe traversing axes. From the post processing of measured data, it is possible to evaluate the dimensional spectrum as well as integral characteristics of the liquid phase such as Sauter mean diameter D_{32} and steam wetness. The CTU optical probe was traversed along the same axes shown in Fig. 1. The informative view of the extinction probe head with the measuring space 13 mm × 50 mm is shown in Fig. 3 [21].

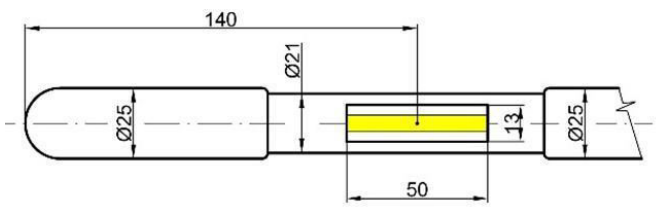

Figure 3: Scheme of optical probe head.

4 Experimental results

Experiments were carried out for three different turbine outputs. For the output of 600 MW it was possible to measure only in plane 2. For the output of 1100 MW and 800 MW measuring took place in plane 0 and 2. Basic parameters of the turbine and the LP part are defined in Table 1. Pressure and temperature at the LP part inlet were read from the turbine control system. Steam wetness in both planes was determined using optical measurements described in this paper.

Table 1: Basic description of measured regimes.

Planes for measurement	Only plane 2		Planes 0 and 2
Turbine output (MWe)	600	800	1100
LP part inlet pressure (MPa)	0.4702	0.5730	0.7288
LP part inlet temperature (°C)	251.1	250.6	249.2
Average wetness measured in plane 0 (1)	–	–	0.0917
Average wetness measured in plane 2 (1)	0.0644	0.0770	0.1270

Comparison of static pressure courses along the blading length for the output of 1100 MW is in Fig. 4. Near the tip ending wall the positive influence of the adjoining diffuser that causes pressure lowering is manifested. The mean channel shows a slight undulation of the pressure profile given by the presence of tie-boss [22] that causes two vortices. They reach up to the 10% of blade length. The influence of tie-boss on efficiency was inves-

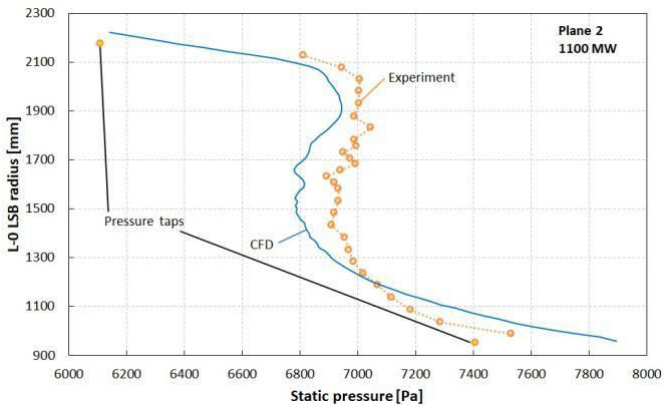

Figure 4: Static pressure course in plane 2 for output of 1100 MW.

tigated in several works [23, 24]. The values of pressure from wall samples do not correspond with pressures determined using pneumatic probe. The reason is mainly a different circumferential position of probe passages (45° above the dividing plane) and pressure samples (15° above the dividing plane). The loss in the exhaust hood and thus the static pressure decreases downwards, towards the condenser. The flow behind the last stage is not circumferentially symmetrical.

Figure 5 shows the courses of wetness in plane 2 from CFD simulation and the experiment for the output of 1100 MW. Here it can be observed that in the last third of the length of the blade, which is the area with the greatest efficiency, the wetness of the steam is high. At the same time, it is possible to observe undulation in the course of wetness behind the tie-boss. Towards the root the wetness decreases, which means that the steam expansion here (even in combination with the highest static pressure) is the least effective.

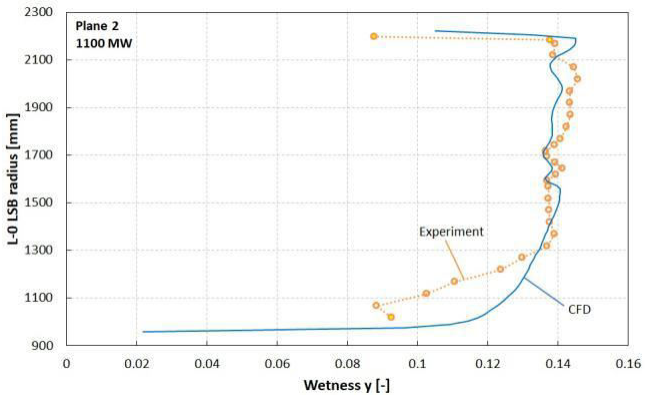

Figure 5: Course of wetness in plane 2 for output 1100 MW.

5 Numerical modelling of steam condensation in steam turbine

5.1 Steam condensation in a steam turbine and condensation model

Due to high rate of expansion steam reaches non-equilibrium subcooled state after exceeding the equilibrium saturation line. The state of steam is characterized by subcooling, ΔT , which is a deviation of the temper-

ature of the metastable vapour phase of the steam from the equilibrium saturation temperature of the steam corresponding to its static pressure ΔT . As the steam continues to expand, its subcooling gradually increases until it reaches the so-called Wilson area. Here, according to the theory of homogenous nucleation in steam, enough stable nuclei of the liquid phase are generated. A nucleation takes place. These nuclei continue to grow due to the condensation of water molecules on their surfaces. The structure of primary water droplets is formed. During this process a considerable amount of heat is released into surrounding steam, which supresses steam subcooling. If the amount of released heat is sufficient, there is a signifi-cant reduction of subcooling and practically no more clusters are formed, only the existing drops grow and the steam approaches equilibrium. The subsequent transition from area with a high rate of expansion and to area with practically zero rate of expansion in the turbine flow part affects the development of the steam subcooling, the intensity of phase transition and the resulting structure of liquid phase of the wet steam.

This complex process of non-equilibrium steam condensation can be described mathematically based on nucleation rate, *J*, and droplet growth rate *dr/dt*. Nucleation rate *J* expresses the number of newly formed droplets of critical radius, r_*, per unit time in a unit volume of steam. Nucleation rate strongly depends on surface tension of water, σ, and droplets critical radius, r_* ($r_* \sim \sigma^2 \Rightarrow J \sim \sigma^3$). The most used relation for nucleation rate is based on the classical nucleation theory corrected by the non isothermic factor ε.

$$J = \frac{1}{1+\varepsilon^s} \sqrt{\frac{2\sigma}{\pi}} \left(\frac{\rho_l}{\rho_g}\right)^2 \exp\left[-K_G \frac{4\pi r_*^2 \sigma}{3kT_g}\right], \quad (1)$$

where ρ_g and ρ_l are densities of vapour and liquid phase of the steam, m_m is molecular weight of water, σ is surface tension of water, r_* is critical radius of droplets, *k* is Boltzmann constant, T_g is temperature of gas phase of steam and K_G is empirical correction coefficient.

When the steam is in the subcooled state, the surface temperature of droplets is higher than the ambient steam temperature. Thus, there is an interphase exchange of heat and mass. As a result, the radius of stable water droplets increases at a rate of *dr/dt*. There are various relations for calculation of droplets growth rate, among the best known is relation according to Gyarmathy [9]

$$\frac{dr}{dt} = \frac{\lambda \Delta T \left(1 - \frac{r_*}{r}\right)}{\rho_l L r (1 + 3.18\mathrm{Kn})}, \quad (2)$$

where λ is thermal conductivity of steam, ΔT is the subcooling of steam defined as $\Delta T = T_l(p) - T_g$, L is specific enthalpy of evaporation at saturation temperature T_g and Kn is Knudsen number, and relation according to Young [25]

$$\frac{dr}{dt} = \frac{\lambda \Delta T \left(1 - \frac{r}{r_*}\right)}{\rho_l L r \left(1 + 2\beta \mathrm{Kn} + 3.78\,(1 - v)\,\mathrm{Kn}\right) \mathrm{Pr}}, \tag{3}$$

where Pr is Prandtl number, β is a free parameter of the model and v is a correction factor defined according to the relation

$$v = \frac{R T_{sat}}{L} \alpha \left(0.5 - \frac{2 - q_c}{2 q_c} \frac{\kappa + 1}{2\kappa} \frac{c_{p\,sat}}{L}\right), \tag{4}$$

where R is the specific gas constant, T_{sat} is the steam saturation temperature, α is an empirical coefficient, q_c is a condensation coefficient, κ is isentropic exponent, and c_p is the isobaric specific heat capacity of vapour.

5.2 Numerical simulation of non-equilibrium steam condensation

In recent years, great progress has been made in numerical simulations of non-equilibrium steam condensation. Presently, the numerical study of condensing steam flows has been extended to 3D with finite-volume/finite-element Navier–Stokes equations, handling the interaction between the vapour and liquid phases using interphase source terms. The Eulerian–Eulerian method, which can simulate low- and high-pressure steam turbines, is widely used to simulate the interaction between the vapour and liquid phases [26]. However, the condensation phenomena involve complex droplet spectra of polydisperse liquid droplets which cannot be modelled using the Eulerian–Eulerian method. Therefore, a moment-based method was also developed for representing polydisperse droplet size distribution [27].

For numerical simulations of non-equilibrium steam condensation both in-house codes and commercial software are used. Ansys CFX is one of the most used software for this purpose [28], where non-equilibrium steam condensation is simulated using the Euler–Euler multiphase method. The basic conservation equations of mass, momentum and energy are extended with simultaneously solved multiphase models and the coupling between the equations is realized via source term formulations. An extended set of

equations is described in detail e.g. in [4]. Steam properties are based on the IAPWS IF-97 standard [29], which includes their formulations for thermo-dynamic metastable region. In Ansys CFX a default condensation model is implemented, which includes a nucleation rate based on the classical nu-cleation theory corrected by a non-isothermal factor and a droplet growth rate by Gyarmathy. It is also possible to modify this 'default' condensation model. The way of customizing the condensation model in Ansys CFX is described in detail in [30].

5.3 The influence of condensation model on the results of numerical simulation of non-equilibrium steam condensation

The conclusion of the international activity "The International Wet Steam Modelling Project" clearly shows that the accuracy of numerical simulation of non-equilibrium steam condensation in Laval nozzles is strongly affected by the choice of condensation model [7]. By setting a suitable condensation model it was possible to reach a good agreement of numerical simulation results with experimental data regardless of the type of numerical solvers. For example, in [30] is shown that the result of numerical simulation car-ried out in Ansys CFX agrees well with the experiment. In this simulation the empirical coefficient K_G in the relation for the nucleation rate is set to 1.3. At the same time the relation by Young [25] is used for droplet growth rate. Similar studies have been done on steam turbines in both fossil and nuclear power plants. Petr and Kolovratnik suggested that for the simu-lation of the complex phenomenon of hetero-homogenous non-equilibrium phase transition in steam operating in real steam turbines it is possible to use with acceptable accuracy the model of homogenous nucleation and they suggested the empirical coefficient K_G in the form [31]

$$K_G = a\,(p_{os})^b\,, \tag{5}$$

where p_{os} means the saturation pressure at the intersection of the expan-sion and steam saturation lines and a and b are adjustable dimensionless parameters.

For the phase transition modelling an in-house code was used based on a 2D statistic approach. To achieve good agreement of measured and mod-eled polydisperse structures of dimensions of primary water droplets both at several points of steam expansion in the turbine (in planes 0 and 2) and for different operating regimes of the turbine, parameters a and b in Eq. (5)

were adjusted. After this adjustment, the correction factor K_G was set to a value greater than 1. It reduces the nucleation rate and thus suppresses the onset of nucleation to the area in which the expanding steam reaches a higher subcooling than would be sufficient for the onset of nucleation using the condensation model with $K_G = 1$.

5.4 Validation of modified condensation model using 2D numerical simulation in Ansys CFX

The in-house code used by Petr and Kolovratnik [31] has a 2D character and does not enable 3D simulation. For this reason, all numerical calculations, the results of which are presented in this paper, are performed in the commercial software Ansys CFX, which uses a different numerical scheme than the internal code by which Peter achieved good agreement with the experimental results. Therefore, it is essential to verify whether the application of the modified condensation model in Ansys CFX also brings a good agreement between the numerical simulation results and the experiment. To validate the modified condensation model numerical simulations of non-equilibrium steam condensation in the 2D section of LP turbine part in its mean radius are performed, see Fig. 6.

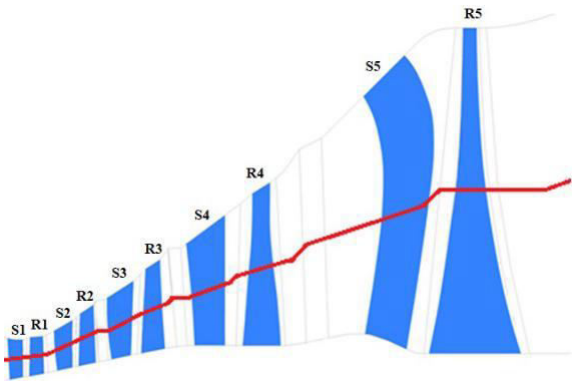

Figure 6: 2D section of LP turbine part in its mean radius.

The calculation model used in simulations is shown in Fig. 7. The calculation model consists of 8 calculation domains. Each calculation domain contains several interblade channels. The numbers of interblade channels in individual domains are determined so that angle at their circumferences equals $\pi/2$. In Fig. 8. a part of the computational mesh is shown. The com-

putational mesh is made using ANSYS TurboGrid. The mesh exclusively consists of hexagonal cells. Specifically, it contains 7.4 million cells.

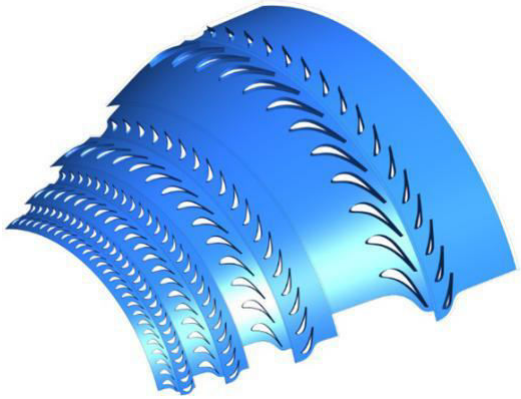

Figure 7: 2D calculation model.

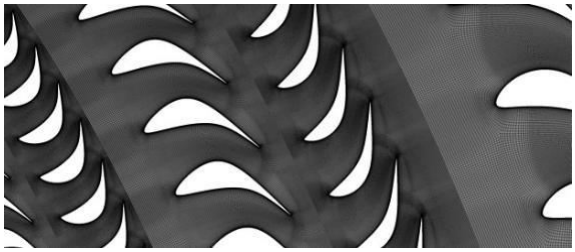

Figure 8: Computational mesh of the 2D calculation model.

Two calculation variants are considered. In the first calculation variant Var_def the steam condensation is modelled using the condensation model that was implemented by default in Ansys CFX. In the second variant Var_CTU a modified condensation model is considered. Both used con-densation models are characterized by the data in Table 2.

Table 2: Description of the calculation models.

Variants	Nucleation rate	Droplet growth rate
Var_def	Classical nucleation theory corrected by non-isothermic factor ε with $K_G = 1$	Gyarmathy relation
Var_CTU	Classical nucleation theory corrected by non-isothermic factor ε with $K_G = a(p_{os})^b$	

At the inlet of the calculation model a ‘pressure-inlet’ boundary condi-tion with total pressure of 0.41 MPa and total temperature of 454.8 K is set at the inlet to L-3 stage. The boundary condition of ‘pressure-outlet’ with static pressure of 0.00704 MPa is set at the model outlet. Regarding the setting of the boundary conditions for the liquid phase, its volume fraction and the number of normalized droplets are set to zero at the inlet of the model. All calculations were carried out in a stationary way and individual calculation domains are connected using the frozen rotor interface model.

In Fig. 9 the contours of nucleation rate are given for both calculation variants. From the comparison of both contours it is evident that the choice of the condensation model has a strong influence on the nucleation process.

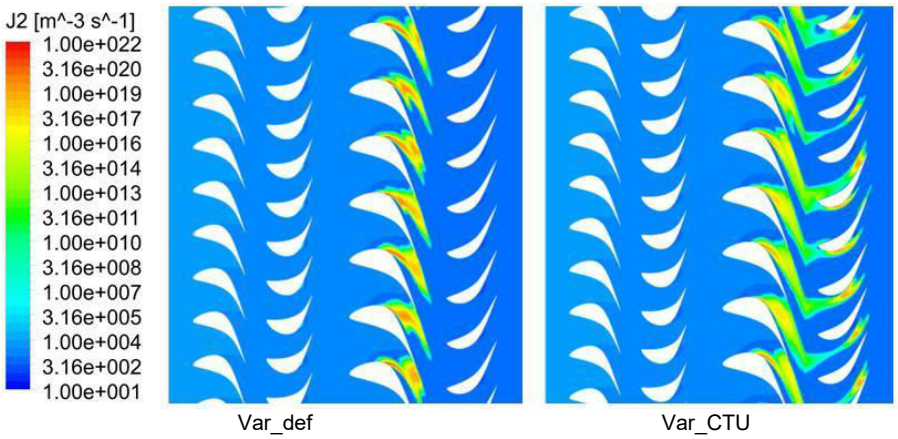

Figure 9: Contours of nucleation rate for Var_def and Var_CTU.

In Fig. 10 for both calculation variants the tangential courses of Sauter mean diameter of droplets D_{32} are given of fine water droplets in two axial positions before and behind the last stage of the turbine where the structure of the wet steam liquid phase was measured using an optical probe.

Var_def Plane 0 and Car_def Plane 2 lines show the courses of Sauter diameter D_{32} of fine water droplets evaluated from the calculation vari-ant where the default condensation model was considered. The Var_CTU Plane 0 and Var_CTU Plane 2 dashlines show the courses of the variant Var_CTU. In both cases dashed lines show tangential courses of Sauter di-ameter of droplets before the last stage. The Sauter diameter values of the fine droplets measured by the optical probe are also displayed by red solid and dotted lines. From the comparison of the results of both calculation

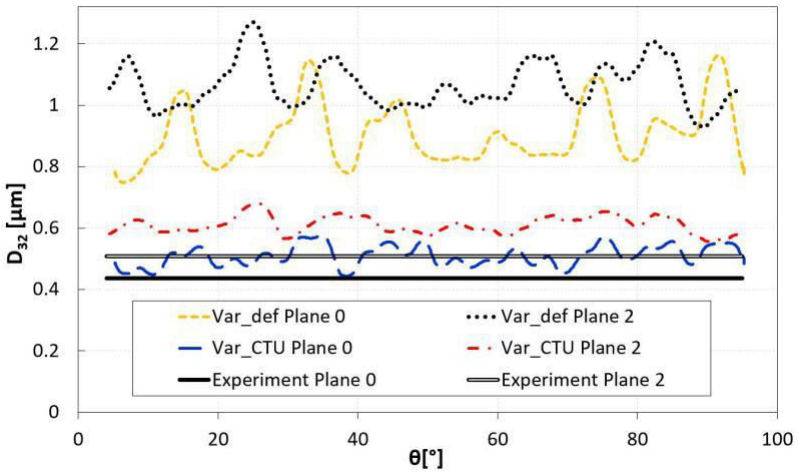

Figure 10: Comparison of measured and calculated Sauter mean diameters.

variants with experimental results it is evident that using modified conden-sation model a better agreement is reached between numerical simulation and experiments.

6 Analysis of thermodynamic wetness loss in LP part of the steam turbine

6.1 Thermodynamic wetness loss

Steam wetness causes erosion problems in steam turbines and at the same time increases energy losses in the turbine. Reduction in turbine efficiency due to additional energy losses by steam wetness has historically been ex-pressed based on the Baumann rule [32]. It says that 1% of stage outlet wetness increases the efficiency by 1%. Moore presents in [33], that in-creasing outlet steam wetness by 1% lowers turbine efficiency by 0.5%. Gyarmathy in his dissertation [9] described the causes of these additional losses using several mechanisms. The most important one is the thermody-namic wetness loss occurring as a result of irreversible inter-phase exchange of mass and heat between the gas and liquid phase of steam during conden-sation (phase transition). This loss is often characterized by the decrease in enthalpy gradient, that is quantified by a volume integral, according to

relation $$\frac{1}{V}\int_V Lm^{\cdot}_{gl}\left(\frac{T_g - T_l}{T_g T_l}\right)^2 dV, \quad (6)$$

where $m^{\cdot}$ is wet steam mass flow, $m^{\cdot}_{gl}$ is interphase mass flux, T_g is steam temperature, T_l is liquid (droplet) temperature, L is specific enthalpy of evaporation, and V is observed steam volume.

6.2 3D numerical simulations of non-equilibrium steam condensation in LP part of the steam turbine

Other CFD simulations were carried out to analyse thermodynamic wetness losses in the steam turbine. The new computational model has 3D character and implies the whole LP part of the turbine. Specifically, the model consists of 5 turbine stages and a diffuser part (see Fig. 6). For non-equilibrium condensation of steam in new 3D numerical simulations, the same settings as for 2D simulations in the previous part of the paper are used.

Three new calculation variants are considered. The first two calcula-tion variants Var1100_def and Var1100_CTU equally respect the nominal operating regime of the turbine with the output of 1100 MW. These vari-ants differ in the used condensation model. The variant Var1100_def uses the condensation model, which is by default implemented in Ansys CFX. The variant Var1100_CTU uses the modified condensation model, which was verified in the previous part of the paper. Other calculation variants Var600_CTU and Var800_CTU respect the operating mode of the turbine with an output of 600 MW and 800 MW, respectively. In both variants the modified condensation model is considered. An overview of all considered calculation variants is given in Table 3.

Table 3: Overview of the new 3D calculation variants.

Variants	Condensation model	Turbine output (MW)
Var1100_def	Default	1100
Var1100_CTU	Modified	1100
Var800_CTU		800
Var600_CTU		600

At the computational model inlet the boundary condition is set of the “pressure-inlet” type with profiles of total pressure and total temperature that correspond with the relevant operating regime. At the computational

model outlet the boundary condition is set of the “pressure-outlet” type with measured static pressure. The computational model consists of 9 com-putational domains. All computational domains contain one inter-blade channel except the last that models a part of the diffuser. The individual computational domains are connected using the stage interface model. All presented calculations are performed as stationary.

Figures 11 and 12 show for variants Var1100_def and Var1100_CTU the nucleation rate contours shown in the periodicities of the selected com-putational domains. The area with the highest nucleation rate is the nucle-ation zone. As it is evident from the comparison of both contours, due to the application of different condensation models the positions of nucleation zone do not coincide for both variants. Specifically, the nucleation zone for Var1100_def is shifted upstream of the position of nucleation zone for

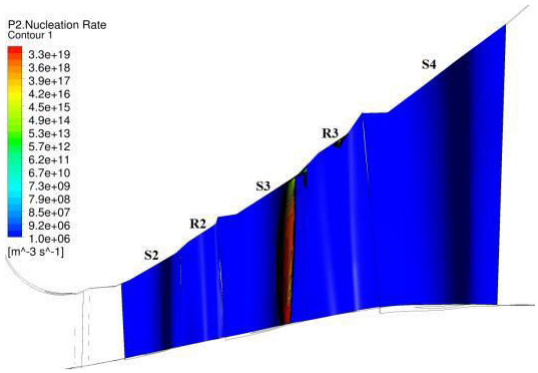

Figure 11: Nucleation rate contours shown in the periodicities for Var1100_def.

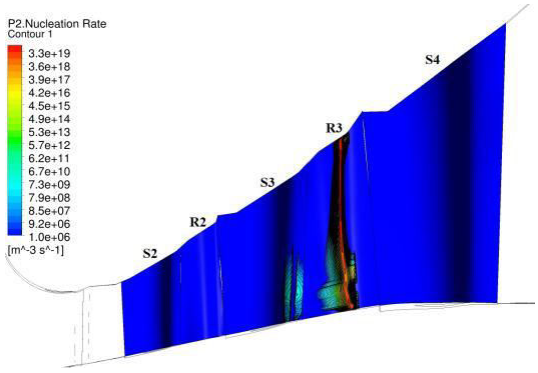

Figure 12: Nucleation rate contours shown in the periodicities for Var1100_CTU.

Var1100_CTU. It means that when using the default condensation model, the nucleation process starts earlier than when using the modified conden-sation model. This confirms the fact that the choice of condensation model can significantly influence the position of the beginning of nucleation pro-cess. The nucleation rate contours for Var800_CTU and Var800_CTU in Fig. 13: show that the turbine operating regimes also affect the position of the nucleation zone.

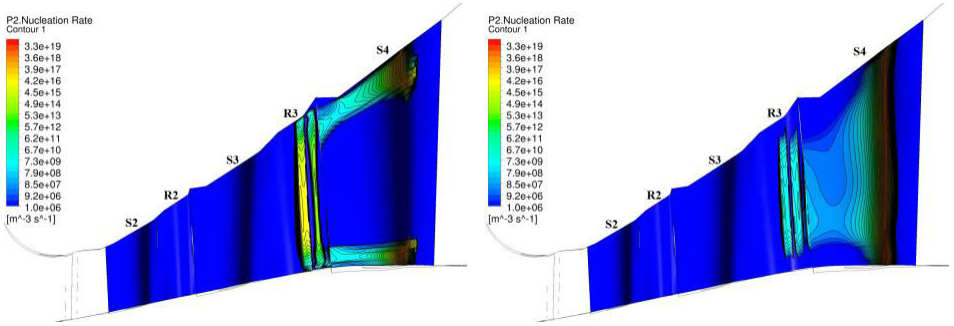

(a) 800 MW (b) 600 MW

Figure 13: Nucleation rate contours shown in the periodicities for Var800_CTU and Var600_CTU.

6.3 Analysis of thermodynamic wetness loss

Figure 14 shows the normalized values of thermodynamic wetness loss Δh_i in the individual rows of blades for the three calculation variants

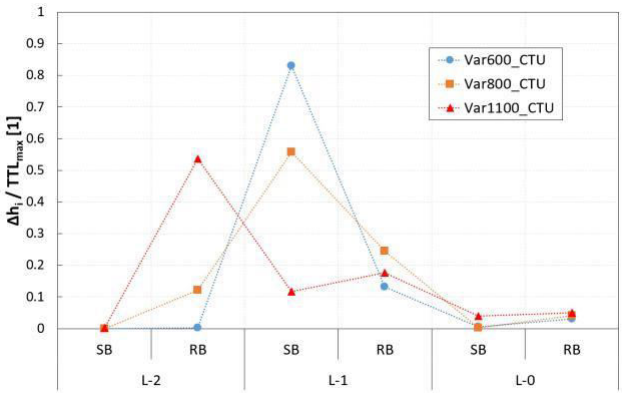

Figure 14: Thermodynamic wetness losses for individual blade rows.

Var600_CTU, Var800_CTU and Var1100_CTU. In the variant with the output of 1100 MW there is an intense nucleation in the rotor blade row of the L-2 turbine stage, which leads to significant thermodynamic wetness losses in this part. Similarly, an intense phase change occurs for the variant with the output of 600 MW in the stator blade row of the L-1 turbine stage. For the variant with the output of 800 MW the nucleation area is divided between rotor blade row of the L-2 stage, where the nucleation starts, and stator blade row of the L-1 stage, where it develops intensively.

Further findings are presented in Fig. 15. Here, for all 4 computational variants the dependences of normalized cumulative thermodynamic wetness losses Δh_i in the individual domains (blade rows, i = 1 to 6) on normal-ized equilibrium steam wetness are given. The equilibrium steam wetness is evaluated based on static pressure of steam expanding in the LP part of the turbine. The distribution of this equilibrium steam wetness in the turbine flow part differs from the distribution of the 'real' non-equilibrium steam wetness evaluated using CFD based on the mass balance of the steam and its liquid phase. It is evident that the thermodynamic wetness loss occurs at non-zero values of equilibrium steam wetness. Specifically, for Var1100_def the thermodynamic wetness loss starts increasing at equilibrium wetness of about 0.7%. Losses for all variants with the modified condensation model start at higher equilibrium wetness. The significant shift in loss onset for Var1100_def compared to other variants is related to the shift of the nu-cleation region of this variant upstream according to the using the default condensation model. In other words, the choice of the condensation model

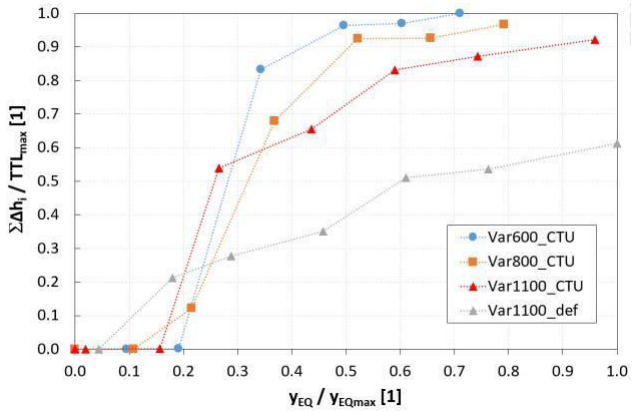

Figure 15: Dependences of normalized total thermodynamic wetness loss (TTL, in kJ/kg) on normalized equilibrium steam wetness.

affects the position of the onset of nucleation and the occurrence of thermodynamic wetness loss.

The comparison of courses of cumulative thermodynamic loss for Var1100_def and Var1100_CTU also shows that the choice of the condensation model also affects the total amount of thermodynamic loss at the end of steam expansion in the turbine. Specifically, for Var1100_def with the default condensation model the total cumulative thermodynamic loss of wetness is lower at the end of expansion than the loss for Var1100_CTU with the modified condensation model. The total thermodynamic wetness loss is also affected by the boundary conditions set in the calculations. This is confirmed by comparison of the loss courses for Var1100_CTU, Var800_CTU and Var600_CTU, in which the same condensation model is considered. However, when calculating these variants, the different operating regimes of the turbine are considered, and therefore different boundary conditions are set for them. These different conditions affect the expansion rate and the maximum achieved steam subcooling in the nucleation zone.

For all loss courses in Fig. 15 a same trend has been observed. The thermodynamic wetness loss increases sharply at the beginning and in the next section of the turbine flow part its growth slows down. However the growth of cumulative loss value will not stop. The initial significant increase in loss is caused by a massive irreversible exchange of mass and heat between steam and stable water nuclei accompanied by subcooling elimination. The subsequent slight increase in thermodynamic wetness loss corresponds with the irreversible exchange of mass and heat between the vapour and liquid phase of steam due to the growth of fine water droplets. In summary, for the variants with the modified condensation model the total cumulative thermodynamic wetness loss increases with a decrease of the turbine output due to deeper steam subcooling.

7 Conclusions

Experimental activities were carried out at the steam turbine in the nuclear power plant at outputs of 600, 800 and 1100 MW, connected with probing the flow field of wet steam before and after the L-0 stage using a pneumatic and optical probe. During the experiments it was possible, among other things, to determine the distribution of static pressure, the spectra of the diameters of primary water droplets and thus the wetness along the blade length of the L-0 stage.

Experimental data were used to fit the condensation model for numeri-cal simulation of non-equilibrium steam condensation in the steam turbine. Specifically, the empirical coefficient for relation for nucleation rate was adjusted according to Petr Kolovratník. The comparison of results of numerical simulation with a modified condensation model with the result of simulation with an unmodified, i.e. by default implemented condensation model in Ansys CFX shows that the course of thermodynamic wetness loss and its total amount sensitively responds to condensation models used in numerical simulations. In particular, the thermodynamic wetness loss for the computational variant with the modified condensation model started with a certain delay compared to the loss course for the variant with the default condensation model. The amount of the total loss at the end of steam expansion in the turbine stages also differs significantly for both computational variants. This fact clearly shows that the quality of numer-ical research of formation and manifestations of wet steam liquid phase in the steam turbine is not sufficient without calibration of the condensation model. However, this step of validation of the condensation model must precede high-quality experimental research into the structure of the liquid phase of the wet steam in the steam turbine.

Acknowledgements The presented work was financially supported by the Technology Agency of the Czech Republic; project TK01020029 “Efficiency Increasing of Turbine Wet Steam Last Stages” and by National Energy Centre TN01000007.

Received 10 June 2021

References

[1] Walters P.T., Skingley P.C.: *An optical instrument for measuring the wetness fraction and droplet size of wet steam flow in LP turbines*. In: Proc. Conf. on Steam Turbines for the 1980s, Vol. 12, London, 9–12 Oct. 1979, C141, 337–348.

[2] Kleitz A., Laali, A.R., Courant J.J.: *Fog droplet size measurement and calculation in wet steam turbines*. In: Proc. Int. Conf. on Technology of Turbine Plant Operating in Wet Steam (J.M. Mitchell, Ed.), London, 11–13 October 1988, 201–206.

[3] Petr V., Kolovratník M.: *Modelling of the droplet size distribution in LP steam turbine*. In: Proc. 3rd Eur. Conf. on Turbomachinery – B, Fluid Dynamics and Thermodynamics, London, 2–5 March 1999, 771–782.

[4] Starzmann J., Schatz M., Casey M.V., Mayer J.F., Sieverding F.: *Modelling and validation of wet steam flow in a low pressure steam turbine*. In: Proc. ASME Turbo Expo 2011, Vancouver, June 6–10, 2011, GT2011-45672, 2335–2346.

[5] Hideaki S., Tabata S. Tochitani N., Sasao Y., Takata R., Osako M.: *Investi-gation of moisture removal on last stage stationary blade in actual steam turbine*. In: Proc. ASME Turbo Expo 2020, virtual, online, Sept. 21–25, 2020, GT2020-14831.

[6] Grübel M., Starzmann J., Schatz M., Eberle T., Vogt D.M., Sieverding F.: *Two-phase flow modeling and measurements in low-pressure turbines – Part I: numerical validation of wet steam models and turbine modeling*. J. Eng. Gas Turbines Power **137**(2015), 4, 042602 (11), GTP-14-1442.

[7] Starzmann J., Hughes F. R., White, A., et al.: *Results of the International Wet Steam Modelling Project*. In: Proc. *Wet Steam Conference*. Prague, Sept. 12–14, 2016.

[8] Fendler Y., Dorey J.M., Stanciu M., Lance M., Léonard O.: *developments for modeling of droplets deposition and liquid film flow in a throughflow code for steam turbines*. In: Proc. ASME Turbo Expo 2012, Copenhagen, June 11–15, 2012, GT2012-68968, 537–547.

[9] Gyarmathy G.: *Grundlagen einer Theorie der Nassdampfturbine*. PhD thesis, ETH Zűrich, Juris-Verlag, Zűrich 1962.

[10] Laali A.R.: *A new approach for assessment of the wetness losses in steam turbines*. In Proc. IMechE Conf. Turbomachinery – Latest Developments in a Changing Scene, London, March, 1991, 155–166.

[11] Wróblewski W, Chmielniak T., Dykas S.: *Models for water steam condensing flows*. Arch. Thermodyn. **41** (2020), 4, 63–92.

[12] Petr V., Kolovratník M.: *Wet steam energy loss and related Baumann rule in low pressure steam turbines*. P. I. Mech. Eng. A-J. Pow. **228**(2014), 2, 206–215.

[13] Holmberg H., Ruohonen P., Ahtila P.: *Determination of the real loss of power for a condensing and a backpressure turbine by means of second law analysis*. En-tropy **11** (2009), 4, 702–712.

[14] Gardzilewicz A.: *Evaluating the efficiency of low pressure part of steam turbines based on probing measurements*. Trans. Inst. Fluid-Flow Mach. **135**(2017), 41–56.

[15] Míšek T., Kubín Z.: *Static and dynamic analysis of 1 220 mm steel last stage blade for steam turbine*. Appl. Comput. Mech. **3**(2009), 1, 133–140.

[16] Luxa M. Safarík P., Synác J., Rudas B.: *High-speed aerodynamic investigation of the midsection of a 48" rotor blade for the last stage of steam turbine*. In: Proc: 10th Eur. Conf. on Turbomachinery Fluid Dynamics and Thermodynamics, ETC10, Lappeenranta, Apr. 15–19, 2013, ETC2013-116.

[17] Finzel C., Schatz M., Casey M.V., Gloss D.: *Experimental investigation of ge-ometrical parameters on the pressure recovery of low pressure steam turbine exhaust hoods*. In: Proc. ASME Turbo Expo 2011, Vancouver, June 6–10 2011, GT2011-45302, 2255–2263.

[18] Jones M., Crossland R.: *performance improvements of nuclear power plants by the application of longer LP last stage blades and advanced design techniques*. In: ASME Power Conf., Baltimore, June 28–31, 2014; POWER2014-32072, V001T04A002.

[19] Hoznedl M., Kolovratník M., Bartoš O., Sedlák K., Kalista R., Mrózek L.: *Experimental research on the flow at the last stage of a 1090 MW steam turbine*. P. I. Mech. Eng. A-J. Pow **232**(2018), 5, 515–524.
[20] Šťastný M.: *Flow field in the last steam turbine stage*. In: Proc. 7th Eur. Conf. on Turbomachinery Fluid Dynamics and Thermodynamics , Euroturbo 7, Athens, March 5–9, 2007, 867–876.
[21] Kolovratník M., Bartoš O.: *CTU optical probes for liquid phase detection in the 1000 MW steam turbine*. In: Proc. EFM14 – Experimental Fluid Mechanics 2014, EPJ Web Conf. **92**(2015), 02035.
[22] Brüggemann C., Schatz M., Vogt D.M., Popig F.: *A numerical investiga-tion of the impact of part-span connectors on the flow field in a linear cascade*. In: Proc.ASME Turbo Expo 2017, Charlotte, June 26–30, 2017, GT2017-63359, V02AT40A005.
[23] Radnic T., Hála J., Luxa M., Šimurda D., Fürst J., Hasnedl D., Kellner, J.: *Aerodynamic effects of tie-boss in extremely long turbine blades*. ASME J. Eng. Gas Turbines Power. **140**(2018), 11: 112604, GTP-17-1218.
[24] Häfele M. Traxinger C., Grübel M., Schatz M., Vog D.M., Drozdowski R.: *Experimental and numerical investigation of the flow in a low-lressure indus-trial steam turbine with part-span connectors*. In: Proc. ASME Turbo Expo 2015: Montreal. June 15–19, 2015, GT2015-42202, V008T26A005.
[25] Young J.B.: *Spontaneous condensation of Steam in Supersonic Nozzles*. 1980STIN...8113306Y, Whittle laboratory, Cambridge University, 1980
[26] Gerber A.G. Kermani M.J.: *A pressure based Eulerian–Eulerian multi-phase model for non-equilibrium condensation in transonic steam flow*. *Int. J. Heat Mass Tran.* **47**(2004), 10–11, 2217–2231.
[27] Hill P.G.: *Condensation of water vapour during supersonic expansion in nozzles*. J. Fluid Mech. **25**(1966), 3, 593–620.
[28] Ansys CFX. https://www.ansys.com/products/fluids/ansys-cfx (accessed 5 March 2021).
[29] The International Association for the Properties of Water and Steam. Revised Release on the IAPWS-97 Industrial Formulation 1997 for the Thermodynamic Properties of Water and Steam. http://www.iapws.org/relguide/IF97-Rev.html (accessed 15 Sept. 2020).
[30] Sova L., Jun G., Šťastný M.: *Modifications of steam condensation model implemented in commercial solver*. AIP Conf. Proc. **1889**(2017), 020039-1–020039-8.
[31] Petr V., Kolovratník M.: *Heterogeneous effects in the droplet nucleation process in LP steam turbines*. In: Proc. 4th Eur. Conf. on Turbomachinery Flud Dynamics and Thermodynamics (G. Bois, R. Decuypere, F. Martelli, Eds.), Firenze, 2001, 783–792.
[32] Baumann K.: *Some recent developments in large steam turbine practice*. J. Inst. Electr. Eng., **59**(1921), 565–623.
[33] Moore M.J.: *Gas dynamics of wet steam and energy losses in wet-steam turbines*. In: Two-Phase Steam Flow in Turbines and Separators (M.J. Moore, C.H. Sieverding, Eds.). Hemisphere, Washington 1976, 59–126.